J. Phys. Chem. A **2005,** *109,* 9443−9455

Asymmetric Indolylmaleimide Derivatives and Their Complexation with Zinc(II)−Cyclen

Başak Kükrer Kaletaş,[†] Hem C. Joshi,[‡] Gert van der Zwan,[‡] Marianna Fanti,[§] Francesco Zerbetto,[§] Kees Goubitz,[||] Luisa De Cola,[†] Burkhard König,*[,⊥] and René M. Williams*[,†]

Molecular Photonic Materials, van't Hoff Institute for Molecular Sciences, Universiteit van Amsterdam, Nieuwe Achtergracht 166, 1018 WS Amsterdam, The Netherlands, Vrije Universiteit, De Boelelaan 1083, 1081 HV Amsterdam, The Netherlands, Dipartimento di Chimica "G. Ciamician", Università of Bologna, via F. Selmi 2, I-40126 Bologna, Italy, Institüt für Organische Chemie, Universität Regensburg, D-93040 Regensburg, Germany, and Laboratory for Crystallography, van't Hoff Institute for Molecular Sciences, Universiteit van Amsterdam, Valckenierstraat 65, 1018 XE Amsterdam, The Netherlands

Received: August 18, 2005

The spectroscopic properties of two asymmetric indolylmaleimide derivatives, 4-bromo-3-(1′*H*-indol-3′-yl)-maleimide and 4-methyl-3-(1′*H*-indol-3′-yl)maleimide, are investigated. The bromo derivative was crystallized and its X-ray structure was determined. Both compounds are strongly colored while their separate components (indole and maleimide) absorb in the UV region only. To understand the ground- and excited-state behavior, the photophysical properties of the two compounds were studied in detail by steady state and time-resolved absorption and emission spectroscopy. Their solvatochromic behavior was investigated by using the Kamlet−Taft approach, which indicates some charge transfer (CT) character in the excited state. Nano- and femtosecond transient absorption spectroscopy was used for the identification and investigation of the CT state. Furthermore, the effect of the complexation with zinc(II) 1,4,7,11-tetraazacyclododecane (Zn-cyclen) on the photophysical properties of these two compounds was studied. An enhancement of the fluorescence intensity upon self-assembly (up to 90 times) and high association constants were observed, which illustrate the potential use of these compounds as luminescent sensors. DFT calculations indicate that HOMO-1 to LUMO excitation is mainly responsible for the charge transfer character and that this transition changes its character drastically when Zn-cyclen complexation occurs, thus giving it sensor properties.

Introduction

The reversible formation of assemblies that results in changes of the photophysical properties, relative to the separate components, is an exciting research area[1−3] where molecular recognition can be used for the design of luminescent sensors[1,4,5] through quenching or enhancement of emission. The concept of chelation-enhanced fluorescence has been used by several research groups[6−12] to design coordinating fluorophores for which the emission quantum yield increases upon the addition of metal ions. This concept was used as an efficient *tool* in analytical detection[13] because the emission enhancement is much more sensitive than the quenching process. Fluorophores based on quinoline,[14] dansyl,[15,16] fluorescein,[17] and anthracene[18] have been reported earlier for these purposes.

The highly fluorescent bisindolylmaleimides are common substructures of natural products,[19] and their biological activity as potent inhibitors of protein kinase C (PKC)[20−22] stimulated their application as lead structures in drug design. The imide function can be used as a coordination site for Lewis acidic zinc azamacrocycles; Kimura and others have studied the ground-state properties of Zn(II) in zinc enzymes with macrocyclic polyamine model complexes, such as *zinc(II) 1,4,7,11-tetraazacyclododecane (Zn-cyclen)*.[23−25] A number of Zn(II) containing azamacrocycles have been used to mimic metallocatalysts in the hydrolysis of carboxyl esters[26] including DNA and ribonucleotides.[27] The complex formation of Zn-cyclen with biologically important imides has also been investigated.[28−30] The coordination of the deprotonated imide nitrogen with the Zn-azamacrocycle has been confirmed by X-ray structures[31] and is believed to be stabilized by hydrogen bonds between the imide oxygen and the NH's of the azamacrocycle.[32] Such a binding motif was also used for the recognition of anions[33] and neutral molecules.[34,29]

The application of imides as red emitting components in organic light-emitting diodes (OLED)[35] as well as potential maleimide-based fluorophores[36] have been reported recently. Despite the huge number of indolylmaleimide derivatives that have been synthesized[20−22,37−42] and used for a broad variety of purposes, very little is known about their photophysical properties. A preliminary report on fluorescence enhancement by complex formation of asymmetrically substituted indole-maleimide systems has recently appeared,[43] as well as some naphthalimide derivatives and their use in fluorescence signaling.[44,45]

We report the spectroscopic properties of two asymmetric indole-maleimide derivatives, 4-bromo-3-(1′*H*-indol-3′-yl)-maleimide (**IM-Br**) and 4-methyl-3-(1′*H*-indol-3′-yl)maleimide (**IM-Me**), see Scheme 1. Furthermore, their noncovalent

---

[*] Corresponding authors. E-mail: B.K., burkhard.koenig@chemie.uni-regensburg.de; R.M.W., williams@science.uva.nl.

[†] Molecular Photonic Materials, van't Hoff Institute for Molecular Sciences, Universiteit van Amsterdam.

[‡] Vrije Universiteit.

[§] Dipartimento di Chimica "G. Ciamician", Università of Bologna.

[⊥] Institüt für Organische Chemie, Universität Regensburg.

[||] Laboratory for Crystallography, van't Hoff Institute for Molecular Sciences, Universiteit van Amsterdam.

10.1021/jp054651z CCC: $30.25

SCHEME 1 Compounds Studied (IM-Br and IM-Me) and Their Complex Formation with Zn-cyclen (IM-R/Zn)

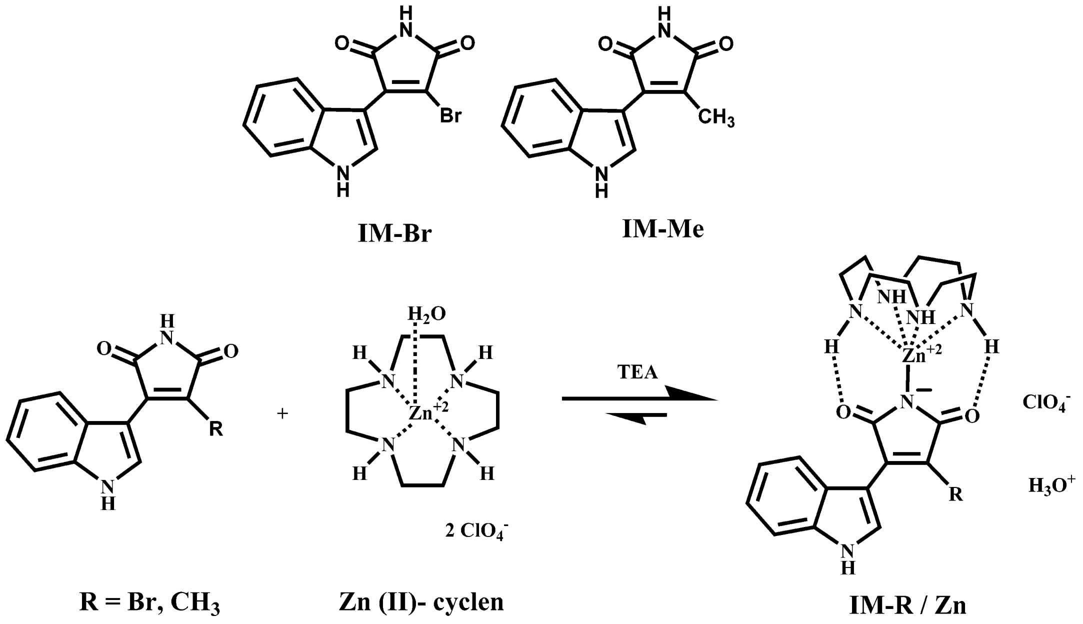

SCHEME 2. Synthetic Route for the Preparation of the IM-Br and IM-Me Compounds

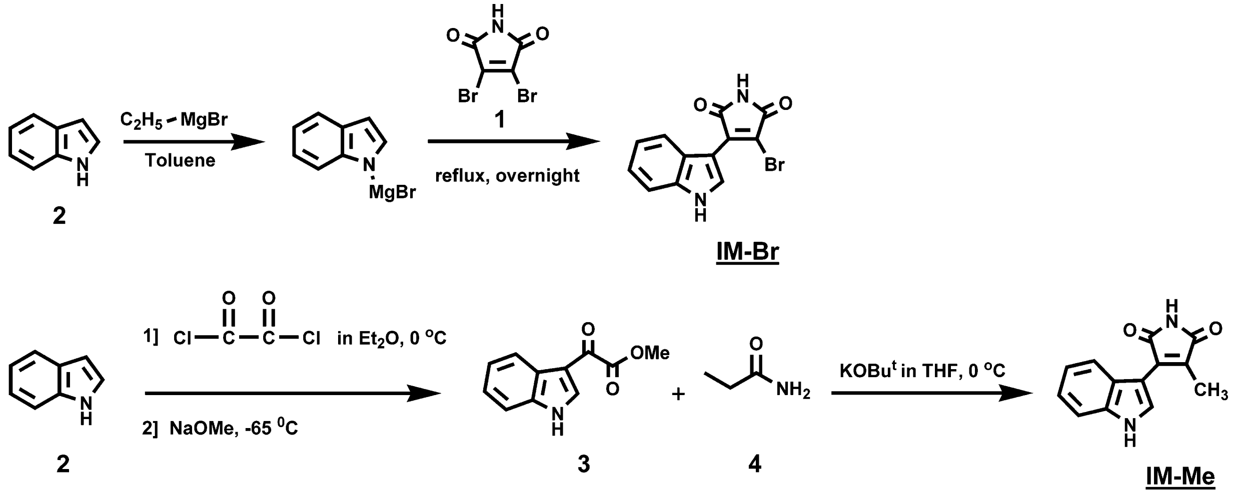

assemblies with Zn-cyclen (zinc(II) 1,4,7,11-tetraazacyclododecane, Scheme 1) are discussed.

Even though the systems look simple, their spectroscopic behavior is rather complicated. To fully characterize the photophysics of the compounds and their assemblies with Zn-cyclen, UV−vis absorption, emission, time-resolved spectroscopy from the nano to the femtosecond time regime and computational analysis have been applied. The **IM-Br** compound was isolated as yellow-orange crystals and X-ray analysis performed.

Results and Discussion

Synthesis of IM-Br and IM-Me. The general preparation of maleimides starts with the corresponding maleic anhydrides that are treated with ammonia or ammonium ions.[46] While the synthesis of symmetric maleic anhydrides and the conversion to the corresponding maleimides are generally high yield reactions, this is not the case for unsymmetrically substituted maleimides.[41]

4-Bromo-3-(1′*H*-indol-3′-yl)maleimide (**IM-Br**) was prepared according to a slightly modified procedure described by Brenner and Faul et al.[47,37] and involves the condensation of an indole Grignard reagent with dibromomaleimide (**1**) (Scheme 2). 4-Methyl-3- (1′*H*-indol-3′-yl)maleimide (**IM-Me**) was prepared according to the general procedure described by Faul et al.[41] by condensation of methylindole-3-glyoxylate (**3**) with propionamide (**4**) using potassium *tert*-butoxide in THF (Scheme 2). The detailed synthetic procedures, including purification and characterization are given in the Experimental Section.

Molecular Structure of IM-Br. Crystals of the **IM-Br** compound were obtained from acetone/hexane solution. The crystal structure of **IM-Br** is given in Figure 1. Selected bond lengths and torsion angles are presented in Table 1. More detailed information about the crystal structure is given in the Experimental Section. It is interesting to notice that the bond between the two chromophoric groups (C4−C6) is single in character. The torsional angle between, e.g., C5−C4−C6−C7 is −32°, indicating that the indole is not coplanar with the maleimide ring, most probably due to the presence of the bulky bromine atom. Since the solid-state structure of this compound reveals that there is a significant torsion angle between the indole and the maleimide unit we expect that the interaction between the two chromophoric units is strongly reduced as compared with a fully conjugated flat structure.

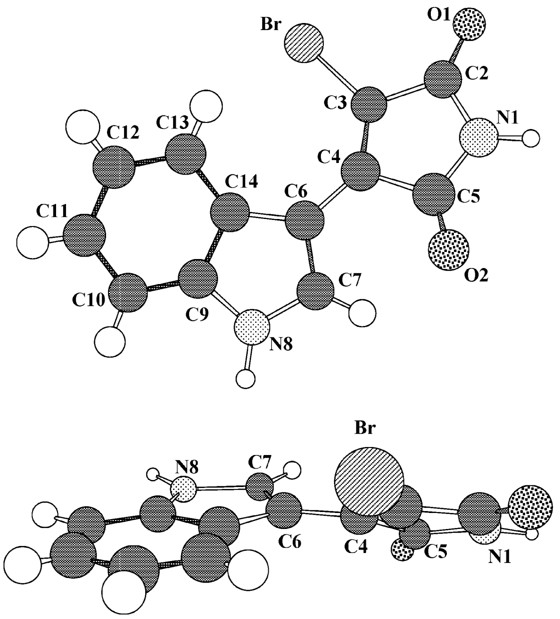

Figure 1. Crystal structure of IM-Br. View from two different sides.

TABLE 1: Selected Bond Lengths (Å) and Torsion Angles (deg) of IM-Br, with Standard Deviations in Parentheses

bonds[a]	values	torsion angles[a]	values
Br−C3	1.861(15)	O1−C2−C3−C4	177.8(18)
O1−C2	1.19(2)	O1−C2−C3−Br	2(2)
O2−C5	1.20(3)	N1−C2−C3−Br	−176.6(11)
N1−H1N	0.9996	N1−C2−C3−C4	−0.5(18)
N8−H8N	1.0026	Br−C3−C4−C6	0(3)
C2−C3	1.49(3)	C3−C4−C6−C14	−33(3)
C3−C4	1.33(2)	C5−C4−C6−C7	−32(2)
C4−C5	1.54(3)	C5−C4−C6−C14	148.2(16)
C4−C6	1.42(2)	C6−C4−C5−O2	−5(3)

[a] See Figure 1.

No suitable crystals for X-ray diffraction could be obtained for **IM-Me**, but we believe that its structure should not deviate considerably from the analogous **IM-Br** derivative.

Steady-State Spectroscopy

As can be seen in Scheme 1, the compounds **IM-Br** and **IM-Me** consist of two units, the well-known electron acceptor maleimide[48−51] and the electron donor indole.[52] For electron donor−acceptor systems a charge transfer can be expected in the ground and/or excited state, which will be reflected in their spectroscopic behavior. In Figure 2, room-temperature UV−vis absorption and emission spectra (inset) of the compounds **IM-Br** and **IM-Me** together with the absorption spectra of the two main chromophoric units, indole and maleimide, are presented. As can be seen from the spectra (Figure 2), the simple components, indole and maleimide, do not show absorption at energy lower than 300 and 325 nm, respectively. Linking them—in a covalent way—results in the compounds **IM-Br** and **IM-Me** and induces mixing of the electronic states, thereby creating other low lying excited states. This gives rise to low energy absorption bands and colored compounds.

For both **IM-Br** and **IM-Me**, the band at 275 nm clearly belongs to the indole $\pi-\pi^*$[53,54] (major contribution) and the maleimide n$-\pi^*$[55,56] (minor contribution) transitions. The absorption bands between 325 and 500 nm characterize the spectra of both compounds. The visible absorption band gives them their distinct orange-yellow color in their solid form as well as new spectroscopic properties. Since the strong electron donor (indole) and electron acceptor (maleimide) character of the two components forming the systems, such broad structureless bands could, in principle, be attributed to $\pi-\pi^*$ transitions with charge transfer (CT) character. The low energy band has a different maximum for the two compounds. In particular, the compound **IM-Br** has a lower energy transition than **IM-Me**. Such behavior can be attributed to the electron donating effect of the methyl group that weakens the electron acceptor ability of the imide unit.

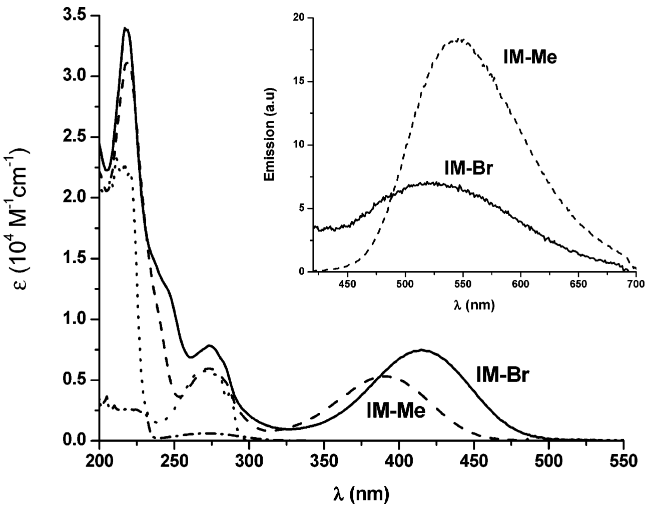

Figure 2. UV−vis absorption spectra of the compounds **IM-Br** (solid), **IM-Me** (dashed), indole (dotted), and maleimide (dash dotted) in acetonitrile. Emission spectra (inset) of **IM-Br** (solid) and **IM-Me** (dashed) in aerated acetonitrile solution, λ_{ex} = 350 nm, corrected for absorption.

TABLE 2: Absorption and Emission Maxima and Emission Quantum Yields (Φ) for IM-Br and IM-Me

	IM-Br			IM-Me		
solvents	λ_{abs}, nm (ϵ)	λ_{em}, nm	Φ	λ_{abs}, nm (ϵ)	λ_{em}, nm	Φ
TOL	417	510	0.072	390	487	0.328
DBE	414	499	0.063	388	477	0.253
DIE	413	500	0.084	385	477	0.277
EA	416	528	0.009	390 (7827)	505	0.086
THF	418	530	0.007	391 (7170)	506	0.0287
DCM	422 (7907)	554	0.014	393 (5111)	528	0.0287
DMF	424 (7528)	543	0.0024	398 (6936)	520	0.0049
EtOH	426 (8229)	535	0.0022	401 (7060)	516	0.0007
ACN	416 (7460)	530	0.0009	390 (5308)	546	0.001

[a] ϵ is the molar extinction coefficient in M^{-1} cm^{-1}. Data are sorted in increasing order of the polarity of the solvents. Key: **Tol**, toluene; **DBE**, dibutyl ether; **DIE**, diisopropyl ether; **EA**, ethyl acetate; **THF**, tetrahydrofuran; **DCM**, dichloromethane; **DMF**, *N*,*N*-dimethylformamide; **EtOH**, ethanol; **ACN**, acetonitrile. Extinction coefficients were only determined in solvents in which the compounds are very soluble.

The structureless emission bands (see Figure 2, inset) were recorded upon excitation into the lowest absorption band of the compounds. Surprisingly, the emission of these asymmetric compounds is extremely weak when compared to symmetric bisaryl-maleimide systems.[43] Absorption and emission maxima (λ_{max}), molar extinction coefficients (ϵ) and emission quantum yields (Φ) were obtained in a series of solvents with different polarities and are summarized in Table 2. When we compare **IM-Br** with **IM-Me**, the latter has higher quantum yields in most of the (nonpolar) solvents. One possible explanation for this result is the heavy atom effect induced by the Br atom in **IM-Br** that promotes intersystem crossing to a low-lying nonemitting triplet state. Another possible explanation is that

TABLE 3: Solvent Parameters and Spectroscopic Data for Compound IM-Br and IM-Me in Various Solvents at Room Temperature[a]

		Kamlet−Taft parameters			IM-Br			IM-Me		
solvents	E_T(30)	π^*	α	β	λ_{abs}, nm	λ_{em}, nm	Δ, cm^{-1}	λ_{abs}, nm	λ_{em}, nm	Δ, cm^{-1}
DBE	33.0	0.24	0	0.46	414	499	4114	388	477	4809
DIE	34.1	0.27	0	0.49	413	500	4213	385	477	5010
TOL	33.9	0.54	0	0.11	417	510	4373	390	487	5107
EtOH	51.9	0.54	0.83	0.77	426	535	4782	401	516	5558
EA	38.1	0.55	0	0.45	416	528	5099	390	505	5839
THF	37.4	0.58	0	0.55	418	530	5056	391	506	5813
ACN	45.6	0.75	0.19	0.31	416	530	5170	390	546	7326
DCM	40.7	0.82	0.30	0	422	554	5646	393	528	6506
DMF	43.2	0.88	0	0.69	424	543	5169	398	520	5895

[a] Data are in increasing order of π^*. The parameter E_T (30), (see text) is in kcal/mol and Δ is the Stokes shift in cm^{-1}.

the lowest excited state in **IM-Br** is a CT level and is a very weakly emitting state. In fact, we would expect a $\pi-\pi^*$ state with charge transfer (CT) character to be the lowest excited state. Whereas the absorption maxima of **IM-Me** and **IM-Br** show only a moderate shift with change of solvent polarity, the emission maxima clearly show a larger solvent dependence. Furthermore, the absorption and emission maxima of **IM-Me** are always hypsochromically shifted compared to **IM-Br** (except for the emission in acetonitrile). The blue shift of the emission maximum upon going from room temperature to 77 K in a butyronitrile matrix (1819 cm^{-1} for compound **IM-Br** and 999 cm^{-1} for **IM-Me**) and the enhancement of the emission quantum yields upon going to nonpolar solvents (see Table 2) also indicates the presence of charge-transfer character in the excited state.

Solvatochromism. Studying the solvent dependence of the spectroscopic properties of the compounds, could lead to an understanding of the nature of their lowest excited states. If a CT character dominates the nature of the lowest excited state, stabilization in polar solvents is expected. When the absorption and emission maxima are compared in Table 2, a red shift in absorption and emission upon going from nonpolar to polar solvents is observed, but the trend is not completely clear and a more complete treatment of the parameters characterizing the solvents was performed using the solvent polarity scale developed in 1976 by Kamlet and Taft.[57] The treatment is based on the use of a multiparameter equation, called *linear solvation energy relationship* (LSER),[58] and its application to similar systems has been recently reported by our group.[43b]

Following this approach, we were able to correlate the spectroscopic properties with the properties of the solvents for a quite good number of solvents. In Table 3, the absorption and emission maxima and the Stokes shifts obtained for **IM-Br** and **IM-Me** are reported in solvents of different polarity and are ordered with increasing value of π^*. As can be seen in Table 3, the absorption maximum undergoes a modest red shift for both compounds upon going from DBE to DMF (from 414 to 424 nm for **IM-Br**, from 388 to 398 nm for **IM-Me**). This indicates a weak CT character in the ground state. However, the emission maxima suggest a stronger charge-transfer character in the excited state. Both the emission maxima and Stokes shifts increase with increasing π^* parameter, which suggest a positive solvatochromic effect.

The following results were obtained by a linear regression analysis of the relation[43b] between the emission maxima of **IM-Br** and **IM-Me** and the independent parameters π^* and α (without taking β into account) by using (see also Figure 3) $XYZ = (XYZ)_0 + s(\pi^*) + a\alpha$.

When the emission maxima of **IM-Br** and **IM-Me** are plotted vs the Kamlet−Taft π^* parameter, similar fits with negative slopes are obtained by using the simpler least-squares regression method:

$$E_{max}(\textbf{IM-Br}) = 59.09\ \text{kcal} - 8.03\pi^*$$

$$R = -0.91, \quad SD = 0.92$$

$$E_{max}(\textbf{IM-Me}) = 62.4\ \text{kcal} - 10.2\pi^*$$

$$R = -0.86, \quad SD = 1.4$$

In either case, the negative coefficients for the π^* values in these equations indicate a positive solvatochromism. As the π^* value of the solvent increases, a red shift for the absorption and/or emission maximum is observed. These results show that the polarizability (π^*) is the major contribution to the observed energy lowering behavior.

For comparison the E_T(30) values are also given in Table 3. The E_T(30) values are based on the properties of the pyridinium *N*-phenolate betaine dye as solvent polarity probe molecule (Reichardt's dye) that shows negative solvatochromism.[61]

In light of these results, we can conclude that the excited state of **IM-Br** and **IM-Me** is strongly polar and has a strong charge transfer character. In particular, if we compare the coefficients of the π^* parameter (see Figure 3) for **IM-Br** (7.6) and for **IM-Me** (9.6), with that of E_T(30) (14.3), and we consider that the latter compound is know to have a strong charge-transfer character.

Complex Formation with Zn(II)-cyclen. The coordination of the imide group with the Zn-cyclen has been intensively studied[34,64,65] and the formation of a bond between the deprotonated imide nitrogen atom and the zinc ion was confirmed by X-ray analyses.[28] To study the assembly process via formation of the coordinative bond between Zn-cyclen and the systems **IM-Br** and **IM-Me**, titration experiments were performed.

Upon addition of stoichiometric amounts of Zn-cyclen to a solution of 2.5 × 10^{-5} mol L^{-1} of **IM-Br**, the formation of the assembly **IM-Br/Zn** (see Scheme 1) was observed in aerated acetonitrile solution. The adduct formation was followed by UV−vis absorption and emission spectroscopy (Figure 4). To favor the deprotonation of the imide to form the Zn-nitrogen bond, a weak base (1 equiv of triethylamine, TEA) was added. Upon addition of the Zn-cyclen, a blue shift (775 cm^{-1}) of the absorption band centered at 416 nm was observed. The shift is accompanied by a decrease of the molar extinction coefficient of the band and by the appearance of a new band in the UV region (Figure 4). The formation of the assembly follows a 1:1 stoichiometry, as determined by a Job plot. The changes in emission properties of **IM-Br** upon binding are even more interesting, since a strong increase in emission intensity was

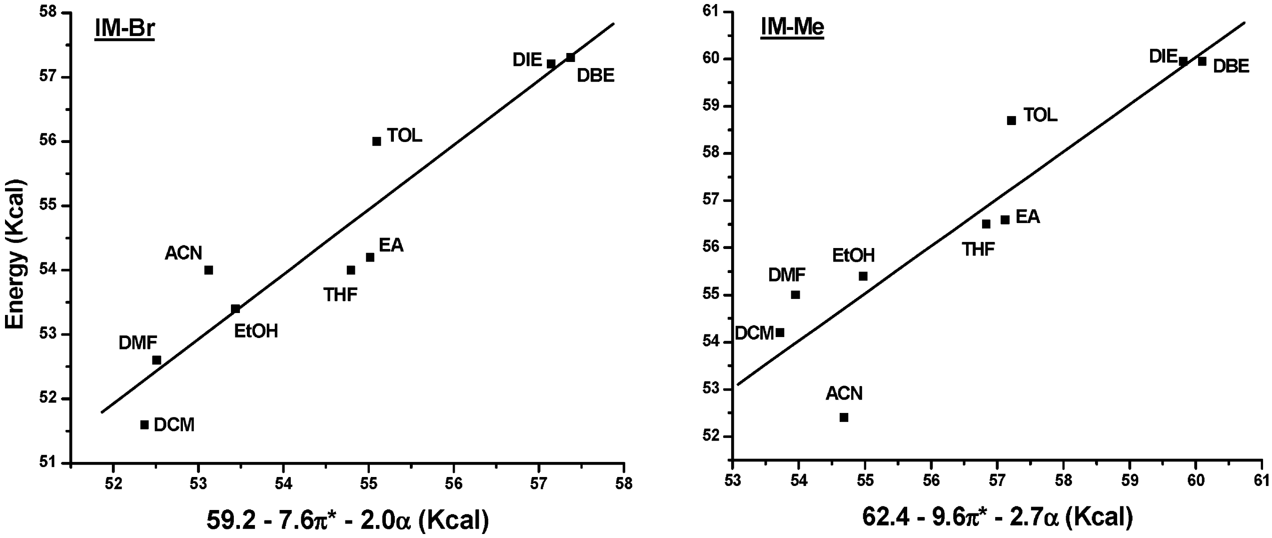

Figure 3. Emission energy maxima of **IM-Br** and **IM-Me** with fit.

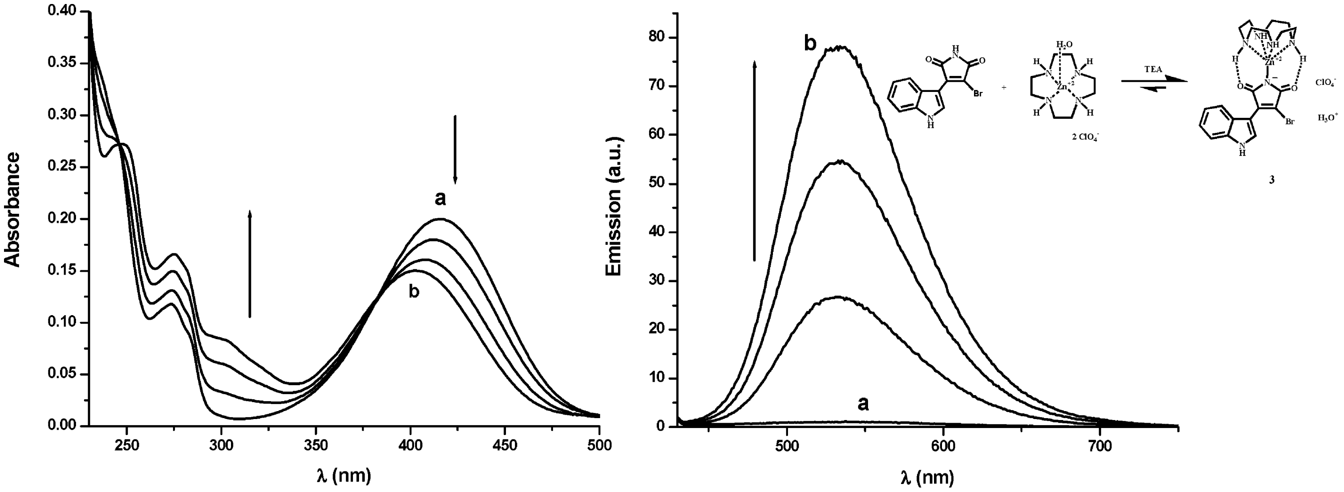

Figure 4. Changes in the absorption (left) and emission (right) spectra of **IM-Br** upon addition of Zn-cyclen in acetonitrile solution. (a) **IM-Br** (2.5×10^{-5} mol L^{-1}), (b) Complex obtained by 1:1 equiv of **IM-Br** and Zn-cyclen in the presence of 1 equiv of TEA.

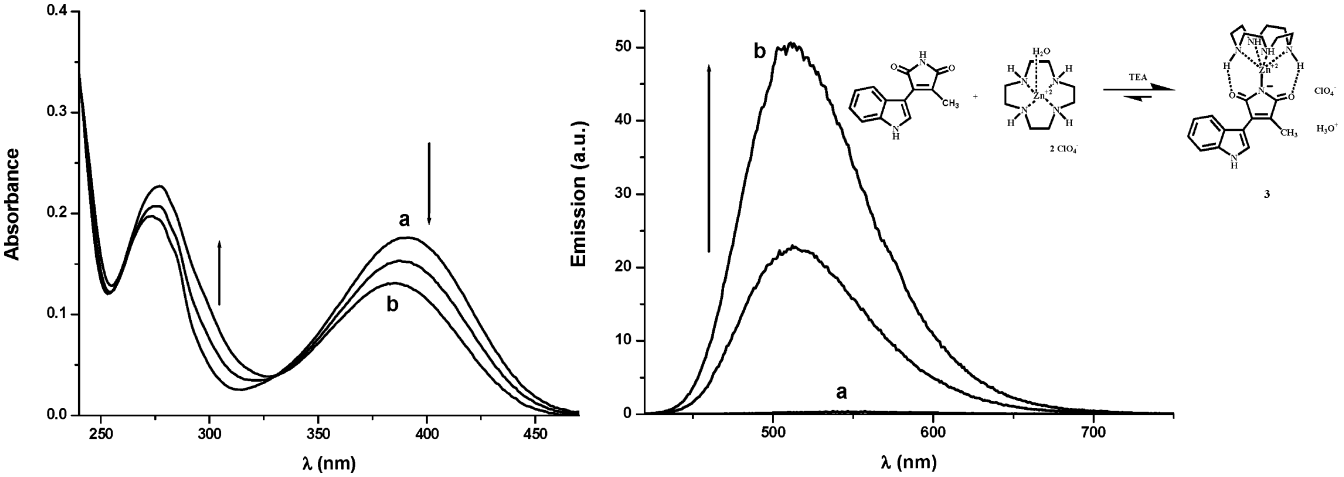

Figure 5. Changes in the absorption (left) and emission (right) spectra of **IM-Me** upon addition of Zn-cyclen in acetonitrile solution (a) **IM-Me** (2.5×10^{-5} mol L^{-1}), (b) complex obtained by 1:1 equiv of **IM-Me** and Zn-cyclen in the presence of 1 equiv of TEA.

observed (see Figure 4). To quantify the emission enhancement, the solution was excited in the isosbestic point (380 nm). The complex formation resulted in a ~80-fold increase in the emission intensity. The association constant calculated by the change in emission is 2×10^6 L mol^{-1}.

Similar titration experiments were performed with **IM-Me** under the same conditions, and adduct formation was followed by UV−vis absorption and emission spectroscopy (Figure 5). The addition of the Zn-azamacrocycle resulted in a blue shift (333 cm^{-1}) of the 390 nm absorption band, similar to what was

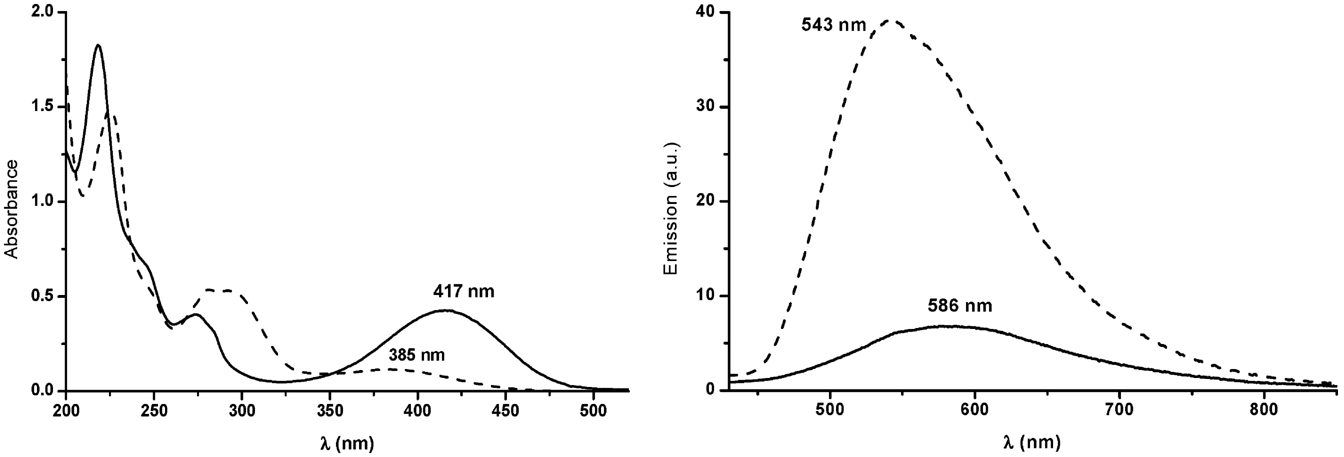

Figure 6. Changes in the absorption (left) and emission (right) spectra (λ_{ex} = 355 nm) of **IM-Br** upon addition of K_2CO_3 in acetonitrile solution. Key: solid line, without K_2CO_3; dashed line, with K_2CO_3.

observed for **IM-Br**. An accompanying decrease in the molar extinction coefficient of this band and a broadening of the UV band at 275 nm indicates the assembly formation (Figure 5). The adduct obtained **IM-Me/Zn** also has a 1:1 stoichiometry. An even stronger increase in emission intensity as compared to the Br analogue, with a blue shift (1107 cm^{-1}) of the maximum was observed for the binding of **IM-Me** with Zn(II)-cyclen. The solution was excited in the isosbestic point (333 nm) and the resulting assembly exhibits an emission that is about 90 times more intense ($\Phi_{\mathbf{IM-Me/Zn}} = 0.09$) than the separate component. The association constant calculated by the change in emission is 1.3×10^6 L mol^{-1}.

To understand whether the spectroscopic changes are due to a more general phenomenon such as the deprotonation of the imide nitrogen, the absorption and emission spectra of **IM-Br** were recorded in acetonitrile solution in the absence and presence of a strong base, potassium carbonate (Figure 6). We also observed an emission enhancement upon coordination with potassium, but the increase was less dramatic

Therefore, we can conclude that coordination with other monovalent Lewis-acid type metal ions could lead to similar results as observed with Zn(II) and such an effect could be used for sensor applications.

Time-Resolved Spectroscopy

Time-resolved spectroscopy was performed to get more information about the nature of the excited states of the individual compounds and of the assemblies with the Zn-azamacrocycle. The emission lifetimes, as well as the emission maxima, are summarized in Table 4.

The excited-state lifetimes of **IM-Br** and **IM-Me** show a trend similar to that of the emission quantum yields (see Table 2). The shorter lifetimes in polar solvents suggests that a deactivation path through a nonradiative state is present for both systems. In some solvents a second decay component is observed for **IM-Br**. If an equilibrium between two excited states is present, the biexponential behavior can be due to the equilibration rate (see below). Upon complexation with Zn-cyclen only a monoexponential decay was detected with a value of 690 ps (see Figure 7). Similar but more dramatic changes in the lifetime were observed for **IM-Me**. The lifetime increased from 120 to 6300 ps upon complexation with Zn-cyclen (Figure 8). Such relatively long emission lifetimes are also observed for the nonassociated maleimide compounds in nonpolar solvents (Table 4) in which the compounds also show relatively high emission quantum yields (Table 2).

TABLE 4: Emission Lifetimes for IM-Br and IM-Me in Several Solvents[c]

	IM-Br		IM-Me	
solvents	λ_{em}, nm	τ_1, τ_2,[a] ns (amp %)	λ_{em}, nm	τ, ns[a]
DBE	499	1.10	477	4.20
DIE	500	1.20	477	4.50
TOL	510	0.98	487	5.40
EtOH	535	0.04	516	*b*
EA	528	0.30 (95), 2.10 (5)	505	3.10
THF	530	0.92	506	0.74
ACN	530	0.03 (97), 0.53 (3)	546	0.12
DCM	554	0.04 (60), 0.64 (40)	528	1.47
DMF	543	0.05 (94), 0.64 (6)	520	0.19

[a] Excitation wavelength is 324 nm. [b] Signal too weak. [c] Data are ordered following the increasing value of the π* parameter of the solvents.

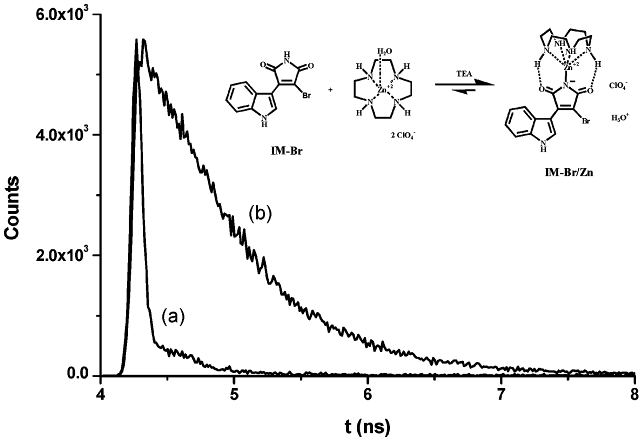

Figure 7. Time-resolved emission for (a) **IM-Br** (τ = 30 and 530 ps) and (b) **IM-Br/Zn** (τ = 690 ps) in aerated acetonitrile solution at room T. λ_{ex} = 420 nm; λ_{det} = 550 nm.

Redox Properties and Cosensitization. To have a complete picture of the possible processes occurring in the systems and to have more evidence of the electronic interactions between the donor and acceptor groups electrochemical and spectroelectrochemical experiments were performed. Unfortunately, the cyclic voltammetry of **IM-Br** in acetonitrile showed irreversible oxidation and reduction processes, independently on the solvent and the electrodes employed. This is not surprising because indole and its monomeric derivatives show irreversible oxidation peaks with a first oxidation occurring at 1.26 V vs SCE.[66] In our case the oxidation peak potential is estimated at 1.43 V and the reduction peak potential at −0.59 V vs SCE. [Cyclic

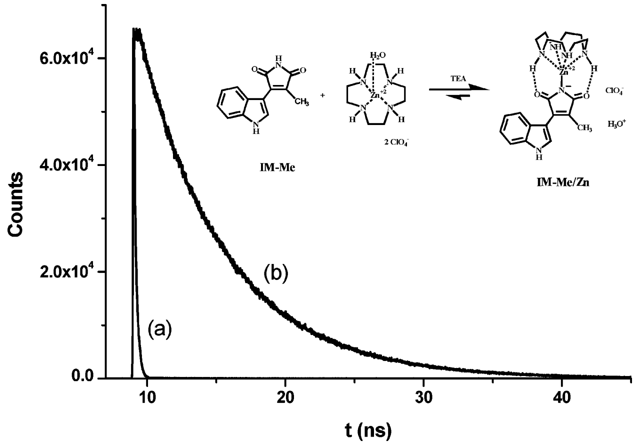

Figure 8. Time-resolved emission of (a) **IM-Me** ($\tau = 120$ ps) and (b) **IM-Me/Zn** ($\tau = 6.3$ ns), in aerated acetonitrile solution at room T. $\lambda_{ex} = 280$ nm; $\lambda_{det} = 520$ nm.

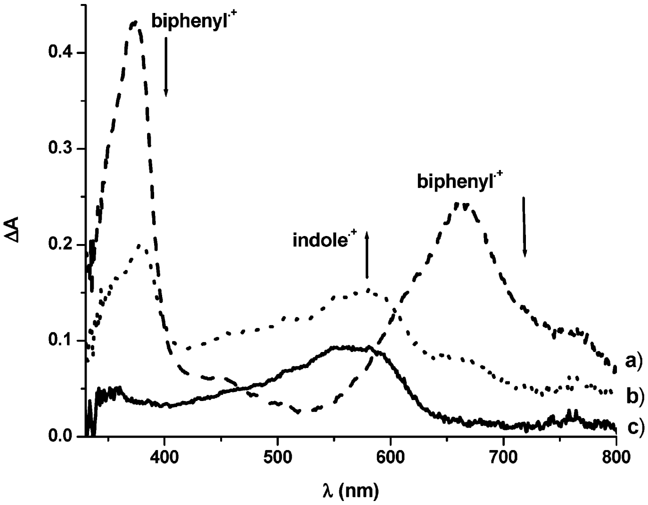

Figure 9. Transient absorption spectra of the radical cation (c) of the indole (indole$^{\bullet+}$) in aerated acetonitrile solution produced using the cosensitization method. Excitation wavelength is 355 nm. Shown are (a) 200 mM biphenyl and 10 mM 1,4-dicyanonaphthalene after 300 ns delay; (b) same as in part a after addition of 1 mM indole at 100 ns delay, and (c) sam as in part a at 300 ns incremental time delay. The transient absorption spectrum c is attributed to the radical cation of indole.

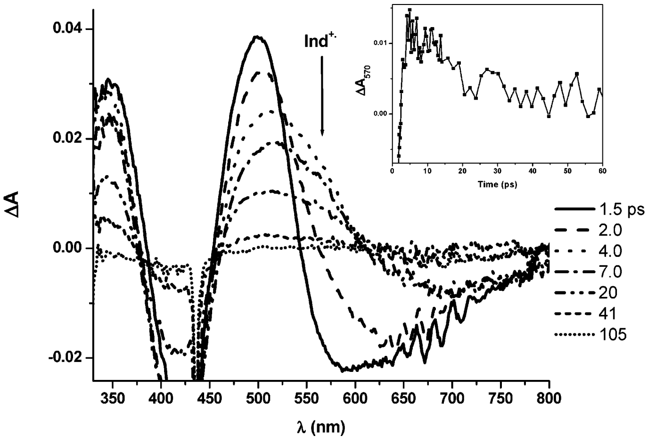

Figure 10. Femtosecond transient absorption spectra of **IM-Br** in aerated acetonitrile solution. Incremental time delays are given on the right. The first four traces show the formation of a CT state absorbing at 570 nm (conditions: A(435 nm) = 1.3, $\lambda_{ex} = 435$ nm, and fwhm = 130 fs). Inset: Kinetic profile of the transient absorption determined at 570 nm.

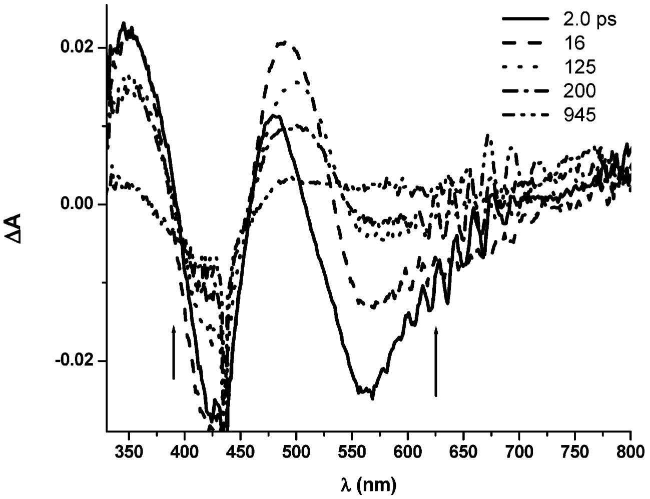

Figure 11. Femtosecond transient absorption spectra of **IM-Br** in aerated THF solution, time delays corresponding to frames are written in the spectra ($\lambda_{ex} = 435$ nm, 130 fs fwhm).

voltammogram ($\nu = 100$ mV s^{-1}) of **IM-Br** (4.9×10^{-4} M) was recorded at a Pt disk electrode in acetonitrile. See Experimental Section for details.] The slightly higher value for the oxidation of the indole can be due to the presence of the electron-withdrawing imide group in the system that makes the compound more difficult to oxidize. The irreversible electrochemical behavior impaired the performance of the spectroelectrochemical experiments.

To gain information about the spectral features of the oxidized indole, the co-sensitization technique[67−69] has been employed. The decay of the radical cation of indole was followed by nanosecond transient absorption spectroscopy (see Figure 9). In this experiment, 1,4-dicyanonaphthalene and biphenyl were used as co-sensitizers (see experimental for details). As can be seen in Figure 9, excitation of 1,4-dicyanonaphthalene at 355 nm created the biphenyl radical cation with absorption bands at 375 and 665 nm.[68] This signal disappeared when indole was added to the solution and a broad signal formed between 520 and 620 nm (Figure 9, parts b and c). Such a new broad band is attributed to the indole radical cation, which can be confirmed by comparison with the data reported in the literature.[70] Therefore, if a charge separation is present upon excitation of our compounds, we should expect the presence of a band with a maximum at about 570 nm due to the absorption of the indole radical cation.

Femtosecond Transient Absorption Spectroscopy. Because of the very short excited-state lifetimes of **IM-Br** and **IM-Me**, transient absorption spectroscopy on the nanosecond time scale did not show any special features. Femtosecond transient absorption measurements were therefore performed to assess the nature and kinetics of the excited states,.

As observed in the steady-state emission for **IM-Br**, there is a change in the properties of this system upon going from nonpolar to polar solvents. For comparison, transient absorption measurements were performed in acetonitrile as a polar medium and in the relatively nonpolar solvent tetrahydrofuran (THF).

The transient absorption spectrum of **IM-Br** is characterized by an instantaneous absorption at 500 nm (attributed to S_1-S_n absorption) and a ground-state bleaching observed at 420 nm. These two features are observed both in acetonitrile (Figure 10) and THF (Figure 11) solutions and are due to the formation of the singlet excited state of the molecule. However the spectrum evolves with not just a simple decay of the bands. An accurate analysis of the spectrum in acetonitrile shows a rise time at

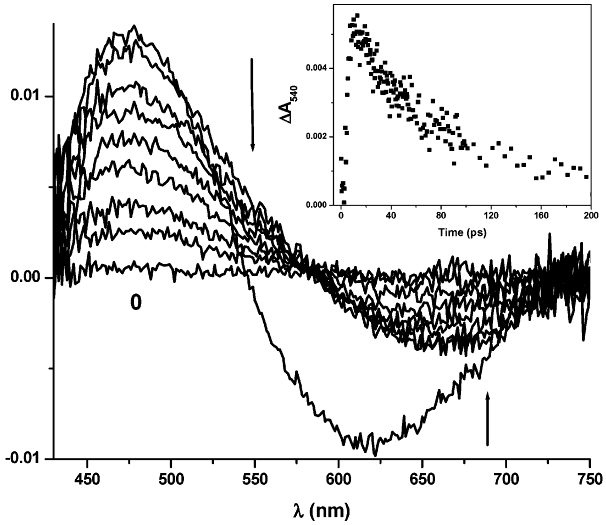

Figure 12. Femtosecond transient absorption spectra of **IM-Me** in aerated acetonitrile solution. Increments are 0, 4, 10, 15, 25, 40, 60, 100, and 150 ps. (λ_{ex} = 390 nm, 130 fs fwhm). Inset: Kinetic profile of the transient absorption determined at 540 nm.

TABLE 5: Decay Times of IM-Br and IM-Me in Acetonitrile Observed by Femtosecond Transient Spectroscopy

	IM-Br[a]			**IM-Me**[b]		
λ_{det}, nm	420	500	570	480	540	640
τ_{rise}, ps	1.0		1.0		1.7	2.0
τ_{decay}, ps	20	1.7/22	27	80	84	72

[a] λ_{ex} = 435 nm. [b] λ_{ex} = 390 nm, in aerated acetonitrile solutions.

570 nm, which is formed within a few picoseconds (1−2 ps) and decays with a time constant of ca. 27 ps (see Figure 10). The latter time constant is in accordance with the short component observed in time-resolved emission spectroscopy. The transient absorption band at 570 nm is assigned to the formation of the radical cation of the indole, the electron-donating component in the system (see Figure 9).

A comparison with the spectra in THF (Figure 11) shows that the positive absorption band at 570 nm is not formed in this solvent. The radical anion of the imide part at 355 nm is not clearly visible because of its low extinction[70] and due to spectral overlap. This result suggests that a fast intramolecular electron-transfer process occurs in the molecule which (due to the low exergonicity; the estimated ΔG in acetonitrile solution is −0.3 eV) is detectable only in polar solvents. These results are in agreement with the higher emission quantum yield in THF (see Table 2) and the fact that the radical cation is not observed in THF.

The femtosecond transient absorption spectra for **IM-Me** were also recorded (see Figure 12). The major observation for this spectrum is the broad transient absorption band between 425 and 525 nm, which has a shoulder like structure around 490 nm. As the emission of **IM-Me** in acetonitrile starts at 450 nm (see Figure 2) there is a strong overlap of the "negative" emission band and the "positive" absorption bands belonging to the radical cation of the indole, expected between 500 and 600 nm. The kinetic analysis performed at 540 nm resulted in 1.7 ps rise time and 84 ps decay. The stimulated emission can be seen between 530 and 750 nm. Probing at 640 nm showed a 2 ps rise time and a 72 ps decay time. The lifetime of **IM-Me** measured with time-resolved emission spectroscopy gave a similar decay value (120 ps).

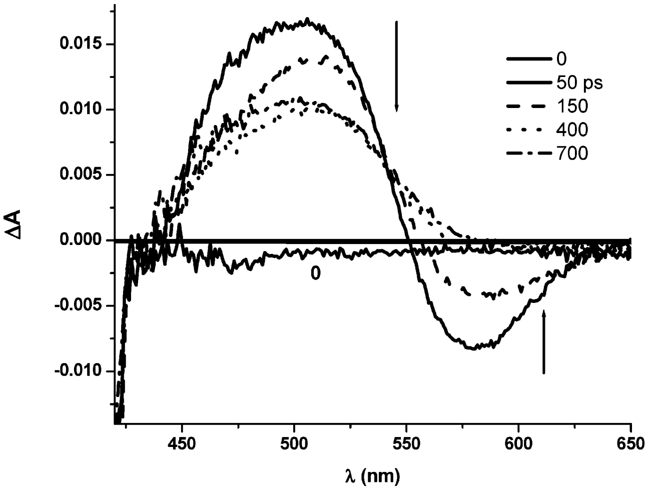

Figure 13. Femtosecond transient absorption spectra of **IM-Br/Zn** (+ 10 μL TEA) in acetonitrile, aerated solution (OD (415) = 0.53, λ_{ex} = 415 nm, 130 fs fwhm).

TABLE 6: Comparison of Calculated and Experimental Main Absorption Peak Positions

	expt,[a] nm	calcd, nm	Δ*E*, cm^{-1}	*μ*,[b] D
IM-Br	417	445	1509	4.31
IM-Me	390	425	2112	4.56

[a] Recorded in **TOL**. [b] Ground-state dipole moments, *μ*.

A summary of the decay times obtained from the kinetic analysis for **IM-Br** and **IM-Me** in acetonitrile, is provided in Table 5.

The femtosecond transient absorption spectrum of the assembly of **IM-Br** with Zn-cyclen was recorded in acetonitrile solution. As can be seen in Figure 13, the shoulder around 570 nm is not observed, and only a strong absorption band at 500 nm is present. The analysis of the kinetics of the decay of both transient signals showed that the ground state is re-formed with a time-constant of 550 ps. This value is in very good agreement with the lifetime measured with single photon counting (690 ps, Figure 7b).

Computational Analysis

Quantum chemical calculations were performed on **IM-Br** and **IM-Me**. Following the structural optimization, the excited states energies and wave functions were calculated and the relevant frontier molecular orbitals were visualized. The molecules were optimized with density functional theory (DFT) at the B3LYP/6-31G* level, using the package Gaussian-98. The nature of the solvent dependency of the photophysical properties suggests that an unraveling of the effects observed experimentally could start from the most straightforward calculation for the isolated molecules.

The electronically excited states were calculated with the time dependent (TD) formulation of density functional theory at the B3LYP/631G* level. The simulation also gives, for each excited state the oscillator strength, f_0, of the $S_0 \rightarrow S_n$ transition. To avoid artifacts and to obtain a more consistent comparison with the experiments, the calculated UV−vis stick spectra were broadened with a Gaussian function (fwhm 2000 cm^{-1}, plots not shown). All the main features of the experimental spectra are well reproduced. Table 6 compares experimental and calculated main absorption peak; the value of the ground-state dipole moments is also indicated.

In Table 7, the energies and the composition of the first two excited states are given, and in Figure 15, the representation of

TABLE 7: Calculated Energies (eV) and Oscillator Strengths (f_0) of the First Two Excited States Together with the Composition of the Wave Function (WF)

molecule	S_1	$f_0(S_1)^a$	S_2	$f_0(S_2)^a$
IM-Br	2.766 eV HOMO → LUMO (0.82)	0.1722	3.228 eV HOMO-1 → LUMO (0.97)	0.0114
IM-Me	2.918 eV HOMO → LUMO (0.85)	0.1465	3.414 eV HOMO-1 → LUMO (0.92)	0.0098

[a] As a rule of thumb, $f_0 = 1$ corresponds to an extinction coefficient of ~50000 L/(mol cm).

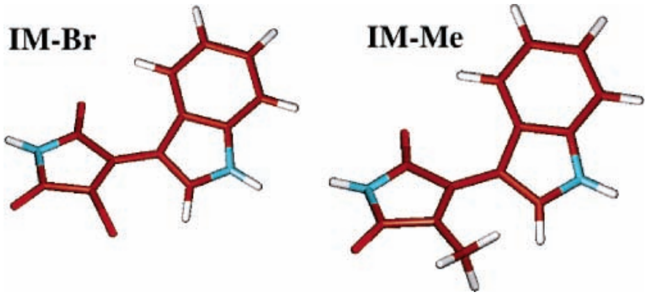

Figure 14. Optimized structures of **IM-Br** and **IM-Me**.

the main molecular orbitals (MO) involved in these excitations is depicted. Analogous calculations were also performed on the deprotonated structure of the bromo derivative, the anionic **IM-Br**$^-$, to simulate the complex with Zn-cyclen. Because of the size of the Zn-cyclen, a direct DFT calculation of the whole system was out of reach. The geometry of **IM-Br**$^-$ was not reoptimized after deprotonation (see Figure 15).

The S_1 state is mainly described as a HOMO → LUMO excitation, with small contributions from other configurations, while S_2 is nearly completely a HOMO-1 → LUMO excitation. Pictorial representation of the orbitals is provided in Figure 15.

A most striking feature of the orbitals is that HOMO-1 of both neutral compounds is fully indole-localized (i.e., on the donor). In the LUMO of **IM-Br** and **IM-Me**, on the other hand, the electron density is mainly (≈ 80%) localized on the maleimide (i.e., on the acceptor) part. Upon HOMO-1 to LUMO excitation, there must be a strong charge transfer from the indole to the maleimide. Notice that the HOMO orbitals are instead entirely delocalized over the molecules.

The observed experimental spectral variations are therefore explained by the solvent-induced shift of S_2, which can become S_1, in the appropriate conditions. The nature of the orbitals also suggests that torsional changes may influence the energy of the electronic excitations that involve the HOMO.

Thus, it is here postulated that in more (polar) solvents the transitions of HOMO-1→LUMO and of HOMO → LUMO become almost iso-energetic and that the former may even become the lowest in energy. The HOMO → LUMO transition corresponds to the emissive $\pi-\pi^*$ excited state described in the experimental part and the HOMO-1 → LUMO transition corresponds to the “dark” charge transfer state (see also next section, Scheme 3).

Interestingly, this interpretation of the MO analysis holds also if we consider the effects of Zn-cyclen complexation on **IM-Br** (or **IM-Me**, see previous sections). Clearly, the HOMO-1 totally changes its character upon deprotonation (=complexation, see HOMO-1 of anionic **IM-Br**$^-$). The charge-transfer character of the HOMO-1 → LUMO transition disappears, and thus the HOMO → LUMO transition corresponding to the formation of the strongly emissive $\pi-\pi^*$ excited-state retains its nature and an 80−90-fold increase of emission is observed experimentally.

We would like to point out that an identical set of calculations has been performed on optimized conformers with the −Br and $-CH_3$ groups in trans position with respect to the N atom of the indole unit (see Figure 1). The qualitative outcome of this second set of calculations is the same as the one described. No substantial difference has emerged, except for some small and expected changes in energy values of MOs and S_n.

Energetic Considerations. The rather complicated spectroscopic properties of these two simple compounds can be explained by the presence of several close lying excited states. It is clear that for both compounds, the emitting excited states are quenched in polar solvents and that the pathway responsible for this quenching is removed upon coordination to the Zn-cyclen moiety.

The experimental and computational results clearly suggest that due to the presence of the electron donor (indole) and an electron acceptor (maleimide) unit, the lowest excited state in polar solvents has a strong charge transfer character. The strongly emissive state observed in nonpolar solvents, is strongly quenched in polar solvents because a charge separated state becomes almost isoenergetic with this emitting state. In a very simple energy diagram (Scheme 3), the charge-separated state can be thermally populated leading to a nonemitting state decaying to the ground state in a few picoseconds (see femtosecond section). Upon deprotonation of the imide for the coordination of Zn-cyclen, the electron withdrawing ability of the imide unit is strongly decreased. In fact, upon deprotonation the imide unit becomes an electron-rich moiety, and this causes a decrease of the oscillator strength of the visible band of the absorption spectrum (see changes in the absorption spectra, Figures 4 and 5). Also the emission spectra for both compounds are strongly affected by the new electronic situation since the charge-separated state cannot be populated anymore (see Scheme 3, parts b and d). For **IM-Br**, the low lying triplet excited state due to the presence of a heavy atom (Br) could represent a further deactivation path for the singlet emitting excited state. Although we have not been able to monitor this triplet state, this involvement would explain why **IM-Me** has a higher emission quantum yield and longer excited-state lifetime than **IM-Br**. It is interesting to notice that, for **IM-Me**, coordination with zinc leads to an even more dramatic emission enhancement than that observed for **IM-Br**. The tentative energy scheme for **IM-Me** is almost identical to the scheme for **IM-Br** but the emitting excited state is higher in energy (~0.12 eV higher), and therefore, the charge separated state can be more easily populated since the process is slightly more exergonic. Upon complexation with the zinc moiety, the emitting state is not quenched anymore and the emission quantum yield increases 80−90-fold for respectively **IM-Br** and **IM-Me**.

Conclusions

UV−vis absorption and steady state and time-resolved emission and transient spectroscopy in several solvents were performed to explain the spectroscopic properties of **IM-Br** and **IM-Me**. The solvatochromic behavior of the compounds was investigated using the Kamlet−Taft solvatochromic parameters and indicates a strong charge-transfer character in the excited

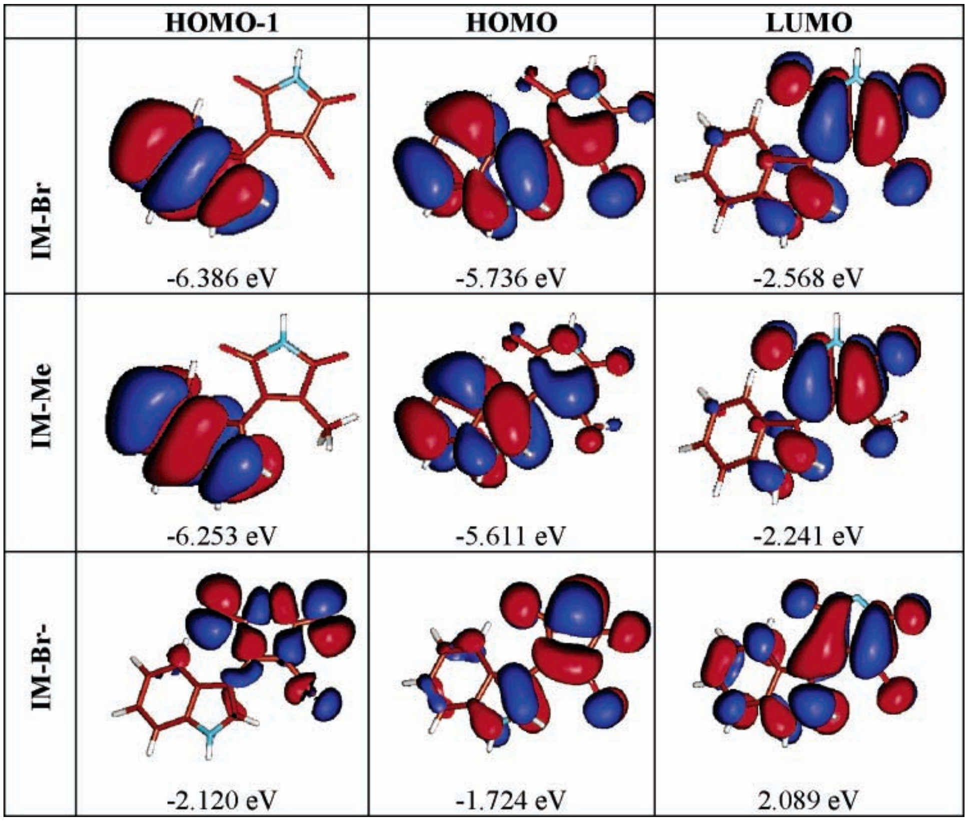

Figure 15. HOMO-1, HOMO, and LUMO of **IM-Br**, **IM-Me**, and anionic **IM-Br**$^-$. MO energies are shown below the orbital representations.

SCHEME 3. Schematic Diagram of the Energy Levels of IM-Br and IM-Me[a]

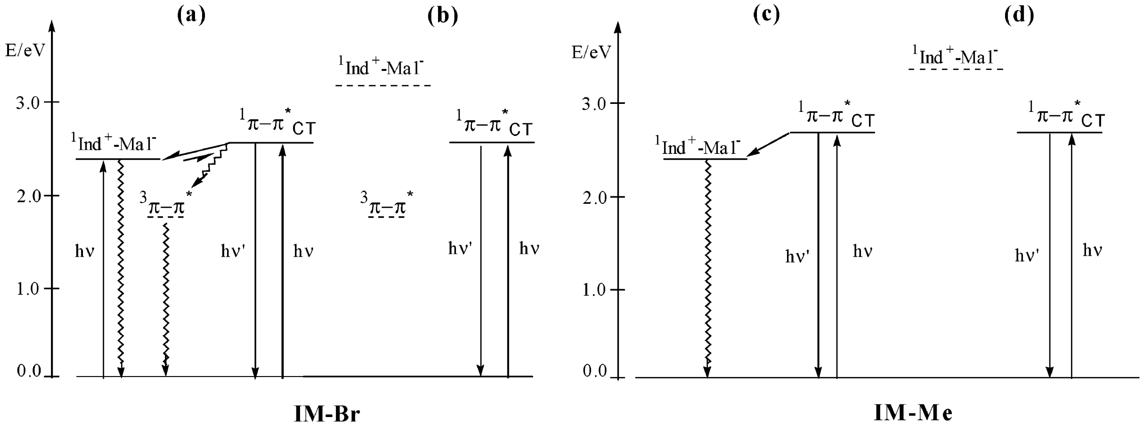

[a] Key: (a) **IM-Br** in polar solvents, (b) **IM-Br** upon coordination by Zn-cyclen (or at low temperature, (c) **IM-Me** in polar solvents, (d) **IM-Me** upon coordination by Zn-cyclen.

state. Additionally, the association constants for the formation of the assemblies with Zn-cyclen were determined using steady-state emission spectroscopy.

The femtosecond transient absorption measurements showed the subpicosecond formation of the charge-separated state in **IM-Br** in acetonitrile. The band formed in a few picoseconds around 560 nm was assigned to the radical cation of the indole unit.

Computational studies support the presence of a charge transfer state close to the first excited singlet state for **IM-Br**. Inspection of the molecular orbitals of **IM-Br** indicates that the charge separation occurs upon HOMO-1 to LUMO excitation. The computational results clearly show that, in the gas phase, HOMO-1 to LUMO excitation is accompanied by a large translocation of electron density from the indole to the maleimide unit, for **IM-Br** and for **IM-Me**. Furthermore, the deprotonation of the imide results in the disappearance of the charge-transfer character of the HOMO-1 to LUMO excitation. These computational results are in excellent agreement with the experimental observations: the quenching of the emission of **IM-Br** upon going to polar solvents has been interpreted as the population of a nonemitting state with substantial charge transfer character. Also the observation that upon going to nonpolar solvents the strongly emitting $\pi-\pi^*$ state starts to dominate for **IM-Me** is in line with these conclusions.

The complexation of **IM-Br** and **IM-Me** with Zn-cyclen is accompanied by a dramatic increase in the emission intensity. Such a strong perturbation introduced by the Zn ion is due to the shift toward higher energy of the charge separated state since the coordination of the metallomacrocycle causes the decrease of the electron accepting ability of the imide part. Asymmetric indolylmaleimide systems have suitable functional groups that can be used in the generation of supramolecular constructions and contain tunable photophysical properties that make them good candidates for molecular sensors.

Experimental Section

Materials. All solvents used were spectroscopic grade and purchased from Acros and Merck Uvasol, and they were used as received unless otherwise indicated. Commercially available deuterated solvents were used as received for the characterization of the compounds. NMR spectra were recorded on a Bruker AC-200 and Bruker AC-300 MHz instrument at ambient temperature. Data were recorded as follows: chemical shift in ppm from internal standard TMS on the δ scale, multiplicity (s = singlet, d = doublet, t = triplet), and assignment. For column chromatography, Merck silica gel 60 was used. TLC was performed on TLC aluminum sheets silica gel 60 F_{254}. Electron impact (EI) and fast atom bombardment (FAB+) mass spectra were carried out using a JEOL JMS SX/SX102A four-sector mass spectrometer. The samples were introduced via the direct insertion probe into the ion source.

All reagents used were obtained from available commercial sources and used without additional purification unless otherwise indicated. The synthesis of 4-bromo-3-(1′*H*-indol-3′-yl)maleimide (**IM-Br**) was took place according to the adapted procedure described by Brenner and Faul et al.[47,37] 4-Methyl-3-(1′*H*-indol-3′-yl)maleimide (**IM-Me**) was prepared according to the adapted procedure described by Faul et al.[41] (1,4,7,11-Tetraazacyclododecane)zinc has been synthesized in the group of Prof. B. König at the University of Regensburg (Regensburg, Germany).

Synthesis. 4-Bromo-3-(1′*H*-indol-3′-yl)maleimide (IM-Br). To an aqueous solution of maleimide (50.4 mg, 5.2 mmol, in 4−5 mL of H_2O) was added 1 mL (19.5 mmol, 6 equiv) of Br_2. The reaction mixture was irradiated (Philips IR 250 W 13352 E/44*3B) for 2−3 h. The precipitated product was filtered off and washed with water and hexane to yield 60% of 3,4-dibromo-maleimide (**1**). ^{1}H NMR (200 MHz, $CDCl_3$): $\delta = 7.26$ (NH, s, br).

To a solution of indole (**2**) (115 mg, 9.8 mmol, 5 equiv) in 16 mL of toluene was added EtMgBr (9.8 mmol, 5 equiv, 9.8 mL of a 1 M solution in THF) under nitrogen atmosphere. After this was heated to 60 °C for 1 h, a solution of 3,4-dibromo-maleimide (**1**) (0.5 g, 1.96 mmol, 1 equiv) in 7 mL of Et_2O and 1.5 mL of THF was added dropwise. The mixture was refluxed (91−94 °C) overnight. The reaction mixture was cooled to room temperature and diluted with 100 mL of ethyl acetate. The organic layer was washed with aqueous 1 N HCl (50 mL), water (50 mL), and brine (50 mL) and dried over $MgSO_4$. The solvent was removed in a vacuum, giving a dark red solid. The crude product was purified by column chromatography (SiO_2, (1) hexane/ethyl acetate 1:1; (2) hexane/ethyl acetate 2:1).

4-Bromo-3-(1′*H*-indol-3′-yl)maleimide (**IM-Br**) was obtained in 40% yield (227 mg) as an orange solid. ^{1}H NMR (200 MHz, DMSO-d_6): $\delta = 12.1$ (s, 1H, NH), 11.4 (s, 1H, NH), 8.06 (d, 1H, aromatic H), 7.94 (d, 1H, $J = 7.4$ Hz, aromatic H), 7.55 (d, 1H, $J = 7.4$ Hz, aromatic H), 7.26−7.11 (2H, complex). MS(EI+): $m/z = 289.9682$ (100%).

X-ray Crystal Structure Determination of IM-Br: $C_{12}H_7BrN_2O_2$, $M_r = 291.1$, orthorhombic, $P2_12_12_1$, $a = 7.483(1)$, $b = 7.636(2)$, $c = 18.212(3)$ Å, $V = 1040.6(4)$Å^3, $Z = 4$, $D_x = 1.86$ g cm^{-3}, λ(Cu Kα) = 1.5418Å, μ(Cu Kα) = 53.2 cm^{-1}, $F(000) = 576$, room temperature, and final $R = 0.087$ for 1390 observed reflections.

A crystal with dimensions 0.05 × 0.20 × 0.80 mm approximately was used for data collection on an Enraf-Nonius CAD-4 diffractometer with graphite-monochromated Cu Kα radiation and a $\omega-2\theta$ scan. A total of 1425 unique reflections was measured within the range $0 \le h \le 9$, $0 \le k \le 9$, and $0 \le l \le 22$. Of these, 1390 were above the significance level of $4\sigma(F_{obs})$. The range of $(\sin\theta)/\lambda$ was 0.055−0.625 Å ($4.9 \le \theta \le 74.6°$). Two reference reflections ([1 1 0], [2 0 3]) were measured hourly and showed no decrease during the 20 h collecting time. In addition, 150 "Friedel" reflections were measured, which were used in the determination of the absolute configuration. Unit-cell parameters were refined by a least-squares fitting procedure using 23 reflections with $40.20 \le \theta \le 43.97$. Corrections for Lorentz and polarization effects were applied. Absorption correction was performed with the program PLATON,[71] following the method of North et al.[72] using Ψ-scans of five reflections, with coefficients in the range 0.440−0.947. The structure was solved by the PATTY option of the DIRDIF99 program system.[73]

The hydrogen atoms were calculated. Full-matrix least-squares refinement on F, anisotropic for the non-hydrogen atoms and isotropic for the hydrogen atoms, keeping the latter fixed on their calculated positions, converged to $R = 0.087$, $R_w = 0.126$, $(\Delta/\sigma)_{max} = 0.88$, and $S = 0.95$. A weighting scheme $w = [25 + 0.01(\sigma(F_{obs}))^2 + 0.0001/(\sigma(F_{obs}))]^{-1}$ was used. The absolute structure parameter[74] refined to $X_{abs} = -0.08$, thus confirming the correct enantiomer. A final difference Fourier map revealed a residual electron density between −2.65 and 2.50 e Å^{-3} in the vicinity of the Br atom. Scattering factors were taken from Cromer and Mann[75] and ref 76. The anomalous scattering of Br was taken into account.[77] All calculations were performed with XTAL3.7,[78] unless stated otherwise.

4-Methyl-3-(1′*H*-indol-3′-yl)maleimide (IM-Me). To a solution of indole (**2**) (2 g, 17.1 mmol) in 20 mL of Et_2O was added oxalyl chloride (1.5 mL, 17.2 mmol) dropwise at 0−5 °C in an ice bath. The solution was allowed to stir for 30 min at that temperature, and the obtained yellow slurry was further cooled to −65−70 °C. Then NaOMe (34.1 mmol, 6.5 mL of a methanol solution; 30 wt %) was added dropwise to this solution. The mixture was allowed to warm to room temperature and was quenched by addition of 10 mL of water. The solid was collected by filtration and washed with water and diethyl ether several times. The product was dried in a vacuum and recrystallized from THF/hexane (1/1) to yield 3.1 g (89%) of methyl indolyl-3-glyoxylate (**3**). ^{1}H NMR (200 MHz, DMSO-d_6): $\delta = 12.43$ (s, NH), 8.48−8.46 (d, 1H), 8.20−8.16 (q, 1H), 7.59−7.53 (m, 1H), 7.37−7.25 (m, 2H), 3.91 (s, 3H).

Methyl indolyl-3-glyoxylate (**3**) (8.2 mmol, 1.66 g, 2 equiv) and propionamide (**4**) (4.1 mmol, 300 mg, 1 equiv) were dissolved in 30 mL of THF and the mixture was cooled to 0 °C. To this solution was added potassium *tert*-butoxide (16.4 mmol, 16.4 mL of a 1.0 M solution in THF, 4 equiv) dropwise, and the mixture was left to stir overnight. After quenching with 8 mL of 35% HCl, the mixture was diluted with ethyl acetate and washed with saturated $NaHCO_3$ solution, and the organic phase was collected and dried over $MgSO_4$. The solvent was evaporated in a vacuum and the crude product was recrystallized from THF/CH_2Cl_2 (1/1) yielding 0.83 g (90%) of 4-methyl-3-(1′*H*-indol-3′-yl)maleimide (**IM-Me**), as a yellow solid. ^{1}H NMR (300 MHz, acetone-d_6): $\delta = 10.96$ (s, NH), 9.58 (s, imide-NH), 7.79−7.75 (s + d, 2H, aromatic H), 7.54−7.51 (d, 1H, aromatic H), 7.24−7.13 (dd, dd, 2H, aromatic H), 2.17 (s, 3H). GC-MS: $m/z = 226$, [100%]; 227, [15.1%]; 228, [2.3%];

155, [71%], (M − C_2O_2NH); 154, [70%], (M − $C_2O_2NH_2$). Calcd for $C_{13}H_{10}N_2O_2$: 226, [100%]; 227, [14.3]; 228, [1.4%].

Instrumental Section

Steady-State Spectroscopy. Electronic absorption spectra were recorded on a Hewlett-Packard UV−vis diode array 8453 spectrophotometer.

Steady-state emission spectra were obtained from a SPEX 1681 Fluorolog spectrofluorometer equipped with two double monochromators (excitation and emission). Emissions are not corrected.Quinine bisulfate solution in 1 N H_2SO_4 (Φ_{em} = 0.546)[79] was used for the emission quantum yield calculations of **IM-Br** in di-*n*-butyl ether, tetrahydrofuran, diisopropyl ether, toluene, diethyl ether, and ethyl acetate solutions. For the solutions in other solvents, $[Ru(bpy)_3]^{+2}$ (Φ_{em} = 0.016 in aerated acetonitrile solution)[80] was used as a standard. For quantum yield of **IM-Me**, quinine bisulfate in 1 N H_2SO_4 solution was used as standard for all solvents.

Cyclic Voltammetry. Cyclic voltammetric scans were performed with a gastight single-compartment cell under an atmosphere of dry nitrogen or argon. The cell was equipped with Pt disk working (apparent surface area of 0.42 mm^2), Pt wire auxiliary, and Ag wire pseudoreference electrodes. The working electrode was polished with a 0.25 μm grain diamond paste between scans. The potential control was achieved with a PAR model 283 potentiostat. The redox potentials are calculated against ferrocene−ferrocenium (Fc/Fc$^+$) redox couple used as an internal standard[81] ($E_{1/2}$ = 0.38 V vs SCE in acetonitrile)[82] and reported in SCE. Tetrabutylammonium hexafluorophosphate (Bu_4NPF_6) was used as the supporting electrolyte.

Time-Resolved Spectroscopy. Time-resolved fluorescence measurements were performed on a picosecond single photon counting (SPC) setup. The frequency doubled (300−340 nm, 1 ps, 3.8 MHz) output of a cavity dumped DCM dye laser (Coherent model 700) pumped by a mode-locked Ar-ion laser (Coherent 486 AS Mode Locker, Coherent Innova 200 laser) was used as the excitation source. A (Hamamatsu R3809) micro channel plate photomultiplier was used as detector. The instrument response (~17 ps fwhm) was recorded using the Raman scattering of a doubly deionized water sample. Time windows (4000 channels) of 5 ns (1.25 ps/channel) to 50 ns (12.5 ps/channel) could be used, enabling the measurement of decay times of 5 ps to 40 ns. The recorded traces were deconvoluted with the system response and fitted to an exponential function using the Fluofit (PicoQuant) windows program.

In the nanosecond pump−probe experiments, for excitation a (Coherent) Infinity Nd: YAG-XPO laser was used. The laser illuminated a slit of 10 × 2 mm. Perpendicular to this, the probe light provided by an EG&G (FX504) low pressure xenon lamp, irradiated the sample through a 1 mm pinhole. The overlap of the two beams falls within the first two millimeter of the cell, after the slit. The probe light from both the signal and the reference channels is then collected in optical fibers which are connected to an Acton SpectraPro-150 spectrograph which is coupled to a Princeton Instruments ICCD-576-G/RB-EM gated intensified CCD camera. Using a 5 ns gate, this camera simultaneously records the spectrally dispersed light from both optical fibers on separate stripes of the CCD.

In the femtosecond transient absorption measurements, a Spectra-Physics Hurricane titanium:sapphire regenerative amplifier system was used as the laser system. The full-spectrum setup was based on an optical parametric amplifier (Spectra-Physics OPA 800) as a pump. A part of the fundamental 800 nm light was used for white light generation, which was detected with a CCD spectrograph. The OPA was used to generate excitation pulses at 345 and 575 nm. The laser output was typically 5 μJ pulse^{-1} (130 fs fwhm) with a repetition rate of 1 kHz. A circular cuvette (d = 1.8 cm, 1 mm, Hellma), with the sample solution, was placed in a homemade rotating ball bearing (1000 rpm), to avoid local heating by the laser beam. The solutions of the samples were prepared to have an optical density at the excitation wavelength of ca. 0.5 in a 1 mm cell. The absorbance spectra of the solutions were measured before and after the experiments, to check for degradation.

Cosensitization experiments were performed with 1,4-dicyanonaphthalene and biphenyl.[68,83,84] The aim of this experiment is to create the radical cation of the donor in a chemical way. For this purpose, 1,4-dicyanonaphthalene was excited at 355 nm. From that an electron is accepted from biphenyl to generate the radical anion of DCN and the radical cation of biphenyl, which readily accepts an electron from the donor compound to create its radical cation as the final step.

The DCN, excited at 355 nm, created the biphenyl radical cation at 375 and 665 nm. This peak, then, quenched when indole was added and a broad signal formed between 520 and 620 nm, which was assigned to the indole radical cation in acetonitrile according to the literature.[70]

Determination of K_{ass} of IM-Br and IM-Me Using Fluorescence Spectroscopy. To a 2.5 mL solution of 2.5 × 10^{-5} M compound and 10 μl TEA of 6.25 × 10^{-3} M in acetonitrile was added a solution of 1.1 × 10^{-3} M of Zn-cyclen in acetonitrile in aliquots of 13.7−27.4 μL (13.7 μL contains 0.25 equiv of Zn-cyclen). The fluorescence spectra were recorded after each addition of Zn-cyclen, while exciting at the isosbestic point, 380 and 333 nm for **IM-Br** and **IM-Me**, respectively. The integral of the emission spectra was plotted against the concentration of the Zn-cyclen, by which the association constant can be calculated.

Acknowledgment. Financial support from NWO (Nederlandse organisatie voor Wetenschappelijk Onderzoek) for the femtosecond equipment and from the UvA (Universiteit van Amsterdam) is gratefully acknowledged.

Supporting Information Available: A .cif file of crystallographic data for **IM-Br**. This material is available free of charge via the Internet at http://pubs.acs.org.

References and Notes

(1) Fabbrizzi, L.; Licchelli, M.; Pallavicini, P.; Sacchi, D.; Taglietti, A. *Analyst* **1996**, *121*, 1763.

(2) Prodi, L.; Bolletta, F.; Montalti, M.; Zaccheroni, N. *Coor. Chem. Rev.* **2000**, *205*, 59.

(3) De Silva, A. P.; Gunaratne, H. Q. N.; Gunnlaugsson, T.; Huxley, A. J. M.; McCoy, C. P.; Rademacher, J. T.; Rice, T. E. *Chem. Rev.* **1997**, *97*, 1515.

(4) Bargossi, C.; Fiorini, M. C.; Montalti, M.; Prodi, L.; Zaccheroni, N. *Coor. Chem. Rev.* **2000**, *208*, 17.

(5) *Fluorescent Chemosensors for Ion and Molecule Recognition*; Czarnik, A. W., Ed.; American Chemical Society: Washington, DC, 1992.

(6) Sousa, L. R.; Larson, J. M. *J. Am. Chem. Soc.* **1977**, *99*, 307.

(7) Ghosh, S.; Petrin, M.; Maki, A. H.; Sousa, L. R. *J. Chem. Phys.* **1987**, *87*, 4315.

(8) Konopelski, J. P.; Kotzyba-Hibert, F.; Lehn, J.-M.; Desvergne, J.-P.; Fages, F.; Castellan, A.; Bouas-Laurent, H. J. *Chem. Commun.* **1985**, 443.

(9) De Silva, A. P.; De Silva, S. A. *Chem. Commun.* **1986**, 1709.

(10) Kollmannsberger, M.; Rurack, K.; Resch-Genger, U.; Rettig, W.; Daub, J. *Chem. Phys. Lett.* **2000**, 363.

(11) Jonker, S. A.; Ariese, F.; Verhoeven, J. W. *J. R. Chem. Soc. Pays-Bas* **1989**, *108*, 109.

(12) Kim, T. W.; Park, J.-H.; Hong, J.-I. *J. Chem. Soc., Perkin Trans. 2* **2002**, 923.

(13) Huston, M. E.; Haider, K. W.; Czarnik, A. W. *J. Am. Chem. Soc.* **1988**, *110*, 4460.

(14) (a) Nasir, M. S.; Fahrni, C. J.; Suhy, D. A.; Kolodsick, K. J.; Singer, C. P.; O'Halloran, T. V. *J. Biol. Inorg. Chem.* **1999**, *4*, 775. (b) Tang, C. W.; Van Slyke, S. A.; Chen, C. H. *J. Appl. Phys.* **1989**, *65*, 3610. (c) Bardez, E.; Devol, I.; Larrey, B.; Valeur, B. *J. Phys. Chem. B* **1997**, *101*, 7786.

(15) Koike, T.; Watanabe, T.; Aoki, S.; Kimura, E.; Shiro, M. *J. Am. Chem. Soc.* **1996**, *118*, 12696.

(16) Prodi, L.; Bolletta, F.; Montalti, M.; Zaccheroni, N. *Eur. J. Inorg. Chem.* **1999**, 455.

(17) Walkup, G. K.; Burdette, S. C.; Lippard, S. J.; Tsien, R. Y. *J. Am. Chem. Soc.* **2000**, *122*, 5644.

(18) Akkaya, E. U.; Huston, M. E.; Czarnik, A. W. *J. Am. Chem. Soc.* **1990**, *112*, 3590.

(19) Steglich, W.; Steffan, B.; Eckhardt, L. K. *Angew. Chem.* **1980**, *92*, 463.

(20) Davis, P. D.; Elliott, L. H.; Harris, W.; Hill, C. H.; Hurst, S. A.; Keech, E.; Kumar, M. K. H.; Lawton, G.; Nixon, J. S.; Wilkinson, S. E. *J. Med. Chem.* **1992**, *35*, 994.

(21) Bit, R. A.; Davis, P. D.; Elliott, L. H.; Harris, W.; Hill, C. H.; Keech, E.; Kumar, H.; Lawton, G.; Maw, A.; Nixon, J. S.; Vesey, D. R.; Wadsworth, J.; Wilkinson, S. E. *J. Med. Chem.* **1993**, *36*, 6.

(22) Hendricks, R. T.; Sherman, D.; Strulovici, B.; Broka, C. A. *Bioorg. Med. Chem. Lett.* **1995**, *5*, 67.

(23) Kimura, E.; Shiota, T.; Koike, T.; Shiro, M.; Kodama, M. *J. Am. Chem. Soc.* **1990**, *112*, 5805.

(24) Kimura, E.; Shionoya, M.; Hoshino, A.; Ikeda, T.; Yamada, Y. *J. Am. Chem. Soc.* **1992**, *114*, 10134.

(25) Koike, T.; Kajitani, S.; Nakamura, I.; Kimura, E.; Shiro, M. *J. Am. Chem. Soc.* **1995**, *117*, 1210.

(26) Kimura, E.; Kodama, A.; Koike, T.; Shiro, M. *J. Am. Chem. Soc.* **1995**, *117*, 8304.

(27) Kalesse, M.; Loos, A. *Liebigs. Ann.* **1996**, 935.

(28) Koike, T.; Gotoh, T.; Aoki, S.; Kimura, E.; Shiro, M. *Inorg. Chim. Acta* **1998**, *270*, 424.

(29) Shionoya, M.; Kimura, E.; Shiro, M. *J. Am. Chem. Soc.* **1993**, *115*, 6730.

(30) Tucher, J. H. R.; Shionoya, M.; Koike, T.; Kimura, E. *Bull. Chem. Soc. Jpn.* **1995**, *68*, 2465.

(31) Shionoya, M.; Ikeda, T.; Kimura, E.; Shiro, M. *J. Am. Chem. Soc.* **1994**, *116*, 3848.

(32) Kimura, E.; Koike, T.; Shiota, T.; Itaka, Y. *Inorg. Chem.* **1990**, *29*, 4621.

(33) Kimura, E.; Aoki, S.; Koike, T.; Shiro, M. *J. Am. Chem. Soc.* **1997**, *119*, 3068.

(34) König, B.; Pelka, M.; Zieg, H.; Ritter, T.; Bouas-Laurent, H.; Bonneau, R.; Desvergne, J.-P. *J. Am. Chem. Soc.* **1999**, *121*, 1681.

(35) Wu, W.-C.; Yeh, H.-C.; Chan, L.-H.; Chen, C.-T. *Adv. Mater.* **2002**, *14*, 1072.

(36) Yeh, H.-C.; Wu, W.-C.; Chen, C.-T. *Chem. Commun.* **2003**, 404.

(37) Faul, M. M.; Sullivan, K. A.; Winneroski, L. *Synthesis* **1995**, 1511.

(38) Faul, M. M.; Sullivan, K. A.; Winneroski, L.; Krumrich, C.; Gillig, J.; Neel, D. A.; Ritto, C. J.; Jirousek, M. *J. Org. Chem.* **1998**, *63*, 1961.

(39) Faul, M. M.; Winneroski, L.; Krumrich, C. *J. Org. Chem.* **1998**, *63*, 6053.

(40) Faul, M. M.; Winneroski, L.; Krumrich, C. *J. Org. Chem.* **1999**, *64*, 2465.

(41) Faul, M. M.; Winneroski, L.; Krumrich, C. *Tetrahedron Lett.* **1999**, *40*, 1109.

(42) Faul, M. M.; Sullivan, K. *Tetrahedron Lett.* **2001**, *42*, 3271.

(43) (a) Kaletas, B. K.; Williams, R. M.; König, B.; De Cola, L. *Chem. Commun.* **2002**, *7*, 776. (b) Kaletas, K. B.; Mandl, C.; van der Zwan, G.; Fanti, M.; Zerbetto, F.; De Cola, L.; König, B.; Williams, R. M. *J. Phys. Chem. A* **2005**, *109*, 6440.

(44) Ramachandram, B.; Sankaran, N. B.; Karmakar, R.; Saha, S.; Samanta, A. *Tetrahedron* **2000**, *56*, 7041.

(45) Ramachandram, B.; Saroja, G.; Sankaran, N. B.; Samanta, A. *J. Phys. Chem. B* **2000**, *104*, 11824.

(46) Davis, P. D.; Bit, R. A.; Hurst, S. A. *Tetrahedron Lett.* **1990**, *31*, 2353.

(47) Brenner, M.; Rexhausen, H.; Steffan, B.; Steglich, W. *Tetrahedron* **1988**, *44*, 2887.

(48) Hoyle, C. E.; Viswanathan, K.; Clark, S. C.; Miller, C. W.; Nguyen, C.; Joensson, S.; Shao, L. *Macromolecules* **1999**, *32*, 2793.

(49) ter Steege, D. H. A.; Buma, W. J. *J. Chem. Phys.* **2003**, *118*, 10944.

(50) Von Sonntag, J. *J. Photochem. Photobiol. A: Chem.* **1999**, *126*, 1.

(51) Von Sonntag, J.; Knolle, W. *J. Photochem. Photobiol. A: Chem.* **2000**, *136*, 133.

(52) Grabowski, Z. R.; Rotkiewicz, K.; Rettig, W. *Chem. Rev.* **2003**, *103*, 3899.

(53) Creed, D. *Photochem. Photobiol.* **1984**, *39*, 537.

(54) Eftink, M. R.; Selvidge, L. A.; Callis, P. R.; Rehms, A. A. *J. Phys. Chem.* **1990**, *94*, 3469.

(55) Seliskar, C. J.; McGlynn, S. P. *J. Chem. Phys.* **1971**, *55*, 4337.

(56) Seliskar, C. J.; McGlynn, S. P. *J. Chem. Phys.* **1972**, *56*, 1417.

(57) Kamlet, M. J.; Taft, R. W. *J. Am. Chem. Soc.* **1976**, *98*, 377.

(58) Abboud, J.-L. M.; Kamlet, M. J.; Taft, R. W. *Prog. Phys. Org. Chem.* **1981**, *13*, 485.

(59) Kamlet, M. J.; Abboud, J.-L. M.; Taft, R. W. *J. Am. Chem. Soc.* **1977**, *99*, 6027.

(60) Kamlet, M. J.; Abboud, J.-L. M.; Taft, R. W. *J. Am. Chem. Soc.* **1977**, *99*, 8325.

(61) Reichardt, C. *Chem. Rev.* **1994**, *94*, 2319.

(62) Kamlet, M. J.; Abboud, J.-L. M.; Abraham, M. H.; Taft, R. W. *J. Org. Chem.* **1983**, *48*, 2877.

(63) Taft, R. W.; Abboud, J.-L. M.; Kamlet, M. J. *J. Org. Chem.* **1984**, *49*, 2001.

(64) Aoki, S.; Sugimura, C.; Kimura, E. *J. Am. Chem. Soc.* **1998**, *120*, 10094.

(65) Kimura, E.; Kitamura, H.; Ohtani, K.; Koike, T. *J. Am. Chem. Soc.* **2000**, *122*, 4668.

(66) Waltman, R. J.; Diaz, A. F.; Bargon, J. *J. Phys. Chem.* **1984**, *88*, 4343.

(67) Brouwer, A. M.; Langkilde, F. W.; Bajdor, K.; Wilbrandt, R. *Chem. Phys. Lett.* **1994**, *225*, 386.

(68) Gould, I. R.; Ege, D.; Moser, J. E.; Farid, S. *J. Am. Chem. Soc.* **1990**, *112*, 4290.

(69) Schaap, A. P.; Siddiqui, S.; Prasad, G.; Palomino, E.; Lopez, L. *J. Photochem.* **1984**, *25*, 167.

(70) Shida, T. *Electronic Absorption Spectra of Radical Ions*; Elsevier Science Publishers, B.V.: Amsterdam, 1988.

(71) Spek, A. L. *Acta Crystallogr.* **1990**, *A46*, C-34.

(72) North, A. C. T.; Phillips, D. C.; Scott Mathews, F. *Acta Crystallogr.* **1968**, *A26*, 351.

(73) Beurskens, P. T.; Beurskens, G.; Gelder, R. d.; Garcia-Granda, S.; Gould, R. O.; Israel, R.; Smits, J. M. M. *The DIRDIF-99 program system, Crystallography Laboratory*, University of Nijmegen: Nijmegen, The Netherlands, 1999.

(74) Flack, H. D. *Acta Crystallogr.* **1983**, *A39*, 876.

(75) Cromer, D. T.; Mann, J. B. *Acta Crystallogr.* **1968**, *A24*, 321.

(76) Cromer, D. T.; Mann, J. B. *International Tables for X-ray Crystallography*; Kynoch Press.: Birmingham, England, 1974; Vol. IV.

(77) Cromer, D. T.; Liberman, D. *J. Chem. Phys.* **1970**, *53*, 1891.

(78) Hall, S. R.; du Boulay, D. J.; Olthof-Hazekamp, R. University of Western Australia: Lamb, Perth, Australia, 2000.

(79) Meech, S. R.; Phillips, D. *J. Photochem.* **1983**, *23*, 193.

(80) Frank, M.; Nieger, M.; Vogtle, F.; Belser, P.; von Zelewsky, A.; De Cola, L.; Barigelletti, F.; Flamigni, L.; Balzani, V. *Inorg. Chim. Acta* **1996**, *242*, 281.

(81) Gritzner, G.; Kuta, J. *Pure Appl. Chem.* **1984**, *56*, 461.

(82) Pavlishchuk, V. V.; Addison, A. W. *Inorg. Chim. Acta* **2000**, *298*, 97.

(83) Mattes, S. L.; Farid, S. *Acc. Chem. Res.* **1982**, *15*, 80.

(84) Majima, T.; Pac, C.; Nakasone, A.; Sakurai, H. *J. Am. Chem. Soc.* **1981**, *103*, 4499.